

Crack arrest in Si_3N_4 -based layered composites with residual stress

M. Lugovy^{a,*}, V. Slyunyayev^a, V. Subbotin^a, N. Orlovskaya^a, G. Gogotsi^b

^a Institute for Problems of Materials Science, National Academy of Sciences of Ukraine, 3 Krzhizhanovsky Str., Kiev 03142, Ukraine

^b Institute for Problems of Strength, National Academy of Sciences of Ukraine, 2 Timiryazevskaya str., Kiev 01014, Ukraine

Received 28 May 2003; received in revised form 17 February 2004; accepted 19 February 2004

Available online 12 April 2004

Abstract

Effect of macroscopic residual stresses on fracture resistance and crack arrest in non-symmetric $\text{Si}_3\text{N}_4/\text{Si}_3\text{N}_{4-x}\text{TiN}$ ($x = 20, 30$ wt%) layered specimens was investigated in this study. One of the aims of the work was also an examination of compliance technique to study R -curve effect as applied to layered specimens. A special attention was paid to the development of an analytical method to calculate fracture resistance – crack length dependence in layered structures having different elastic moduli of layers. The validity of the method and its application were examined by calculating stress intensity coefficients for edge-cracked layered specimens and comparison of the results with mechanical characteristics obtained from bending test.

© 2004 Elsevier Ltd. All rights reserved.

Keywords: A. Layered structures; B. Fracture toughness; Modelling; C. Crack; Residual stress

1. Introduction

Multilayered ceramic matrix composites (MCMC) have a wide variety of applications in modern technology. Layers comprising ceramic materials are extensively used in engineering structural components with the objective to improve the mechanical, thermal, chemical and tribological performance. Recent research and development in the area of MCMC seek to utilize such materials in such diverse applications as surface coatings, thermal barrier protection for turboengines, valves in reciprocating engines for automobiles and cutting tools.

Despite of many attractive properties such as high hardness and high temperature stability, MCMC have the major disadvantage of lacking reliability and sensitivity to surface contact damage. The last factor can lead to strength decreasing and even to catastrophic failure.

A number of strategies have been developed in recent years to design tough and strong MCMC [1]. These include designing weak interfaces for crack deflection [2], using residual compression in surface layers [3], pro-

moting crack bifurcation effect in compressive layers [4], controlling the frontal shape of the transformation zones in zirconia ceramics [5]. These mechanisms should provide an arrest of cracks in layered structure, increasing consequently its reliability. The reliability of the MCMC can be improved also by controlling the size of flaws introduced into the material during processing. This may be achieved by dispersion of a slurry of the designated power and by its passing through a filter. As a result only heterogeneities with sizes smaller than a critical size can pass through, depending on the filter fineness. Drawback of this procedure is its expensiveness and that such material is still subject to damage during machining with the reliability degraded accordingly.

In multilayered materials with strong interfaces the differences in the coefficients of thermal expansion (CTE) between dissimilar materials or phase transformation in layers inevitably generate thermal residual stresses during subsequent cooling [6]. The essential feature of residual stress distribution in a layered structure is that it arises on a macroscopic scale. The relative thickness of different layers determines the relative magnitudes of compressive and tensile stress, while the magnitude of the strain mismatch between the layers dictates the absolute values of the residual stresses.

* Corresponding author. Fax: +44-380-444-2131.

E-mail address: lugovy@viptelecom.net (M. Lugovy).

Control of the thermal stresses and the accompanying changes in structure are important to ensure the structural integrity of the layered component during manufacturing and in service.

A key feature that imparts good mechanical properties in the multilayer systems is the ability to be toughened significantly by placing their surfaces in residual compression and to arrest crack. It was shown in [3] that a residual surface compression of ~ 500 MPa in a surface layer of three-layered alumina–zirconia specimen can increase its fracture toughness by a factor of 7.5 (up to $30 \text{ MPa m}^{1/2}$) for edge-crack lengths of the order of the surface-layer thickness. The toughening derived from macroscopic surface compression was in fact a crack shielding phenomenon and the fracture toughness increasing was equivalent to a crack growth resistance (R) behavior [7]. The R -behavior is often connected with bridging mechanism. The mechanism is associated with the closure stress field that acts behind the tip of the advancing crack [8]. However, there are some differences in R -behavior resulted from bridging mechanism (this is typical for non-layered ceramics) and from the shielding phenomenon in layered structures. First, while bridging mechanism gives rise to dependence of fracture resistance only on crack length increment, the shielding effect results in the dependence of fracture resistance on overall crack length [3,7,9]. Second, the bridging mechanism promotes an increasing fracture resistance with crack advance whereas the shielding effect can induce both increasing and decreasing of fracture resistance depending on crack tip location in tensile or compressive layer.

Actually layered specimen fracture resistance measured experimentally is the apparent fracture toughness. This is due to superposition of different effects like residual stress shielding and structure in-homogeneity. In fracture mechanics one usually includes stresses in the crack driving force; however it is sometimes useful to consider residual stresses as part of the crack resistance. Thus the higher resistance to failure for layered structure with residual stress is obtained from a reduction of the crack driving force rather than an increase in the intrinsic material resistance to crack extension [9].

Despite of numerous experimental and theoretical studies of fracture resistance of MCMC, systematic researches of R -behavior and of crack arresting in layered composites are very scarce. A great number of publications are dealing with symmetrical layered structure. This is an idealized situation. Really laminates are characterized by some dissymmetry of their architecture due to random deviations in fabrication process. Besides specific non-symmetrical layered structures are important in some engineering applications. Conventional analytical consideration of shielding effect in laminate also neglects the difference between elastic moduli of layers [3,7]. However, effect of different moduli on fracture resistance of laminates is not so negligible. The

influence of elastic modulus variation across a layered sample on R -curve behavior is investigated in [10]. It was shown that the elastic moduli difference affects residual stress distribution and has consequently a significant influence on the measured R -curve behavior. But detailed analysis of conditions of crack arresting, its stable/non-stable growth was not carried out in [10].

The effect of macroscopic residual stresses on fracture resistance and crack arresting in non-symmetric Si_3N_4 -based layered structures fabricated in the form of single-edge-V-notch-bend (SEVNB) specimens is investigated in this study. One of the aims of this work is also an examination of compliance technique to study R -curve effect as applied to layered specimens. A special attention is paid to the development of an analytical method to calculate fracture resistance – crack length dependence in layered structures having different elastic moduli of layers. The validity of the method and its application are examined by calculating stress intensity coefficients for edge-cracked layered specimens and comparing the results with the mechanical characteristics obtained from bending test data.

2. The model

Fig. 1 shows a schematic of the two-component multilayer specimen analyzed in this study. Parameter t_i designates thickness of layer number i . The total thickness of specimen of rectangular cross-section is w , its width is b , the total number of layers is N . Choice of coordinate system is important for further consideration. It is the most appropriate to put the coordinate origin on tensile surface of bending specimen. The geometry of the multilayered material analyzed here is such that the problem can be reduced to one dimension, and that analytically tractable solutions can be used. Here, the parameters of interest in the study of mechanical behavior depend only on x -coordinate.

It was shown in [3,11] that the stress intensity factor, K_1 , due to an arbitrary stress distribution in the pro-

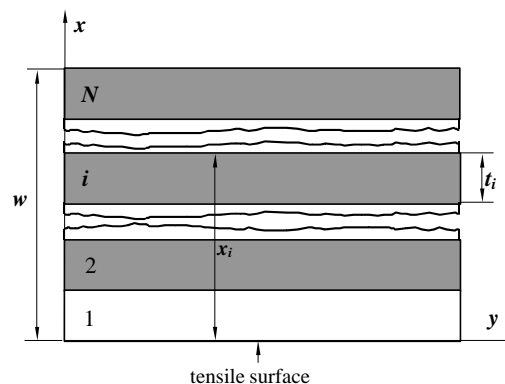


Fig. 1. Schematic of the two-component multilayer specimen.

spective path of the crack in the absence of the crack $\sigma(x)$, can be obtained as

$$K_1 = \int_0^a h\left(\frac{x}{a}, \alpha\right) \sigma(x) dx, \tag{1}$$

where x is the distance along the crack length measured from the surface for an edge crack, a is the crack length, $\alpha = a/w$, w is the specimen thickness (Fig. 2). Note that the distance along the crack length coincides with x -coordinate in coordinate system chosen. For edge-cracked specimens, Fett and Munz [11] have developed the following weight function:

$$h\left(\frac{x}{a}, \alpha\right) = \frac{(2/\pi a)^{1/2}}{(1 - \frac{x}{a})^{1/2} (1 - \alpha)^{3/2}} \times \left[(1 - \alpha)^{3/2} + \sum A_{v\mu} \left(1 - \frac{x}{a}\right)^{v+1} \alpha^\mu \right]. \tag{2}$$

The values of the coefficients $A_{v\mu}$ and the exponents v and μ in (2) are listed in Table 1.

In a case when deformation is a function of coordinate x only, it follows from strain compatibility [12] that overall deformation $\varepsilon(x)$ must be linear for elastic material:

$$\varepsilon(x) = \varepsilon_0 + kx. \tag{3}$$

Here ε_0 is the deformation at $x = 0$, k is the specimen curvature. An equal biaxial stress state is known to be the most appropriate approximation to describe stress state in real layered specimens [13]. This is the case for infinite dimensions along y - and z -directions, but with finite value of specimen thickness. In the equal biaxial stress state we have: $\varepsilon(x) = \varepsilon_{zz} = \varepsilon_{yy}$, $\sigma(x) = \sigma_{zz} = \sigma_{yy}$, where ε_{zz} , ε_{yy} , σ_{zz} , σ_{yy} are strain and stress components

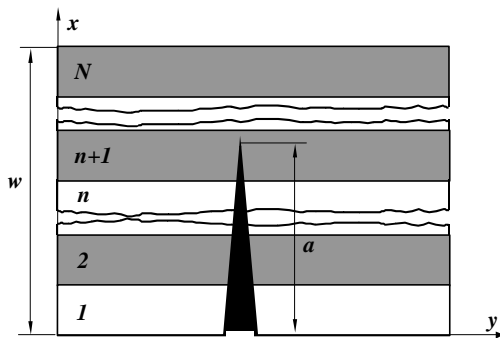


Fig. 2. Schematic of analyzed crack location in layered specimen.

along z - and y -axis, respectively. Edge effects (occurrence of three-dimensional stresses near the edges of layered composite over a distance from the edge which is approximately equal to the layer thickness [14]) can be neglected due to their high-localized character. Then

$$\sigma(x) = E'(x)[\varepsilon(x) - \tilde{\varepsilon}(x)], \tag{4}$$

where

$$E'(x) = E(x)/[1 - \nu(x)]. \tag{5}$$

In Eqs. (4) and (5), $E(x)$, $\nu(x)$ are the elastic modulus and Poisson ratio distributions along x -axis. $\tilde{\varepsilon}(x)$ is the strain non-associated with stress. It is associated with thermal expansion or/and with a volume change due to a crystallographic phase transformation.

The static balance conditions [12] in chosen coordinate system result in a system of linear equations with unknown values ε_0 and k :

$$\begin{cases} F_a + \int_0^w b\sigma(x, \varepsilon_0, k) dx = 0, \\ M_a + \int_0^w bx\sigma(x, \varepsilon_0, k) dx = 0, \end{cases} \tag{6}$$

where F_a is the applied axial force, M_a is the applied bending moment. Solution of the system is [13]

$$\varepsilon_0 = \frac{-I_2(J_0 - F_a/b) + I_1(J_1 - M_a/b)}{I_1^2 - I_0I_2}, \tag{7a}$$

$$k = \frac{I_1(J_0 - F_a/b) - I_0(J_1 - M_a/b)}{I_1^2 - I_0I_2}, \tag{7b}$$

where

$$I_j = \int_0^w x^j E'(x) dx \quad (j = 0, 1, 2), \tag{8}$$

$$J_j = \int_0^w x^j \tilde{\varepsilon}(x) E'(x) dx \quad (j = 0, 1). \tag{9}$$

Note that superposition principle is valid for this problem. It permits to express the stress variation along the path of the crack in a specimen as

$$\sigma(x) = \sigma_a(x) + \sigma_r(x), \tag{10}$$

where $\sigma_a(x)$ is the bending stress in the prospective path of the crack in the absence of any residual stress, $\sigma_r(x)$ is the residual stress distribution.

In [3] the bending stress $\sigma_a(x)$ was expressed as follows:

$$\sigma_a(x) = \sigma_m \left(1 - \frac{2x}{w}\right), \tag{11}$$

Table 1
Values of coefficients $A_{v\mu}$ in Eq. (2) [11]

v	$\mu = 0$	$\mu = 1$	$\mu = 2$	$\mu = 3$	$\mu = 4$
0	0.498	2.4463	0.07	1.3187	-3.067
1	0.54165	-5.0806	24.3447	-32.7208	18.1214
2	-0.19277	2.55863	-12.6415	19.763	-10.986

where σ_m is the applied stress on tensile surface of bending specimen. It is well known that

$$\sigma_m = \frac{1.5Ps}{bw^2} = \frac{6M_a}{bw^2}. \tag{12}$$

Here P is the critical load (applied bending load corresponding to specimen failure), s is the support span. However, the differences in the elastic moduli of the layers were not taken into account in [3]. Really different elastic moduli of the layers result in specific distribution of applied stress along x -direction. Elastic material demonstrates continuous linear distribution of applied stress under bending. This promotes piecewise-linear distribution of applied stress, shown schematically in Fig. 3. To derive applied stress distribution under bending we can use expressions (3), (4), (7a), (7b) and (12), taking into account that in this case $F_a = 0$. We can take $\tilde{\varepsilon}(x) = 0$ if applied stress acts only. Then it follows that applied stress acting in the layer with number i is

$$\sigma_a(x) = \frac{E'_i w^2}{6(I_{L1}^2 - I_{L0}I_{L2})} \sigma_m [I_{L0}x - I_{L1}], \quad x_{i-1} \leq x \leq x_i. \tag{13}$$

Here x_i is the coordinate of upper boundary of i th layer. $E'_i = E_i/(1 - \nu_i)$, E_i and ν_i are the elastic modulus and Poisson ratio of layer number i , respectively. I_{Lj} can be obtained from expression (8) accounting for layered structure (Fig. 1)

$$I_{Lj} = \frac{1}{j+1} \sum_{i=1}^N E'_i (x_i^{j+1} - x_{i-1}^{j+1}) \quad (j = 0, 1, 2). \tag{14}$$

Residual stress distribution can be found from Eqs. (3), (4), (7a) and (7b), taking into account that $F_a = 0$, $M_a = 0$ (Fig. 3):

$$\sigma_r(x) = \frac{E'_i}{I_{L1}^2 - I_{L0}I_{L2}} [I_{L1}J_{L1} - I_{L2}J_{L0} + (I_{L1}J_{L0} - I_{L0}J_{L1})x], \quad x_{i-1} \leq x \leq x_i, \tag{15}$$

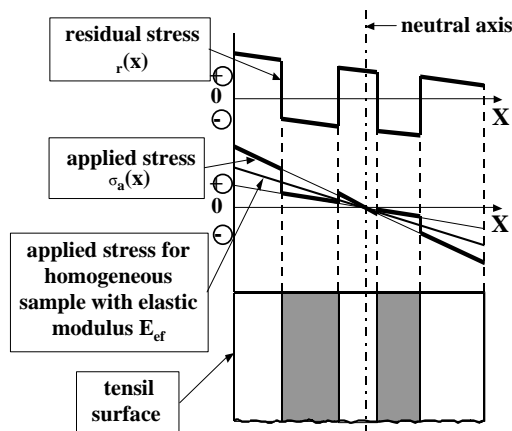


Fig. 3. Schematic of residual and applied stress distribution in layered specimen.

where J_{Lj} can be obtained from the expressions (9) accounting for layered structure

$$J_{Lj} = \frac{1}{j+1} \sum_{i=1}^N \tilde{\varepsilon}_i E'_i (x_i^{j+1} - x_{i-1}^{j+1}) \quad (j = 0, 1). \tag{16}$$

Here $\tilde{\varepsilon}_i$ is the strain of i th layer non-associated with stress. The thermal expansion or/and a volume change due to a crystallographic phase transformation can be the source of this strain, however, the case of phase transformation is out of the scope of this paper. In case of thermal expansion $\tilde{\varepsilon}_i = \int_{T_0}^{T_j} \beta_i(T) dT$, where $\beta_i(T)$ is thermal expansion coefficient of i th layer at temperature T ; T_0, T_j are actual and joining temperature, respectively. Joining temperature is determined as the temperature at which the layers constituting the material are joined. If $\beta_i(T)$ is a linear function, $\tilde{\varepsilon}_i = \langle \beta_i \rangle \Delta T$, where $\Delta T = T_j - T_0$, $\langle \beta_i \rangle = [\beta_i(T_0) + \beta_i(T_j)]/2$ is the average value of thermal expansion coefficient in temperature range from T_0 to T_j .

Using the condition of crack growth ($K_1 = K_{1c}$, K_{1c} is the fracture toughness of the layer which embeds the crack tip) and (1), (10), we obtain

$$K_{1c} = \int_0^a h\left(\frac{x}{a}, \alpha\right) \sigma_a(x) dx + \int_0^a h\left(\frac{x}{a}, \alpha\right) \sigma_r(x) dx. \tag{17}$$

Using Eq. (13) the first integral in (17) can be expressed for a layered material as

$$\int_0^a h\left(\frac{x}{a}, \alpha\right) \sigma_a(x) dx = \frac{\sigma_m w^2}{6(I_{L1}^2 - I_{L0}I_{L2})} \times \left\{ E'_{n+1} \int_{x_n}^a h\left(\frac{x}{a}, \alpha\right) [I_{L0}x - I_{L1}] dx + \sum_{i=1}^n E'_i \int_{x_{i-1}}^{x_i} h\left(\frac{x}{a}, \alpha\right) [I_{L0}x - I_{L1}] dx \right\}, \tag{18}$$

where n is the number of layers broken by the crack (or notch) completely (Fig. 2). Using Eq. (15), the second integral in (17) for a layered material takes the form

$$K_r = \int_0^a h\left(\frac{x}{a}, \alpha\right) \sigma_r(x) dx = \frac{1}{I_{L1}^2 - I_{L0}I_{L2}} \left\{ E'_{n+1} \int_{x_n}^a h\left(\frac{x}{a}, \alpha\right) \times [I_{L1}J_{L1} - I_{L2}J_{L0} + (I_{L1}J_{L0} - I_{L0}J_{L1})x] dx + \sum_{i=1}^n E'_i \int_{x_{i-1}}^{x_i} h\left(\frac{x}{a}, \alpha\right) \times [I_{L1}J_{L1} - I_{L2}J_{L0} + (I_{L1}J_{L0} - I_{L0}J_{L1})x] dx \right\}. \tag{19}$$

K_r is the stress intensity due to the residual stresses.

The following formula is given for the stress intensity of an edge crack in the specimen under bending as being accurate to $\pm 0.2\%$ in the range $\alpha = 0$ to 1 [15]:

$$K_1 = \frac{Ps}{bw^{3/2}}f_0(\alpha), \tag{20}$$

where $f_0(\alpha)$ is a non-dimensional stress intensity coefficient given by the following expression [15]:

$$f_0(\alpha) = \frac{1.5\alpha^{1/2}[1.99 - \alpha(1 - \alpha)(2.15 - 3.93\alpha + 2.7\alpha^2)]}{(1 + 2\alpha)(1 - \alpha)^{3/2}}. \tag{21}$$

Taking into account Eqs. (12) and (21), expression (20) can be transformed to the form

$$K_1 = Y(\alpha)\sigma_m a^{1/2}, \tag{22}$$

where

$$Y(\alpha) = \frac{1.99 - \alpha(1 - \alpha)(2.15 - 3.93\alpha + 2.7\alpha^2)}{(1 + 2\alpha)(1 - \alpha)^{3/2}} \tag{23}$$

It was shown in [3] that Eqs. (20) and (22) can be successfully used to determine fracture toughness of ceramic matrix layered materials. However, it should be noted that as applied to inhomogeneous (particularly, layered) materials the equations give so-called apparent fracture toughness. In bending test this is the fracture toughness of some effective homogeneous specimen that meets the following conditions: (1) to have the same dimensions as real layered specimen; (2) to have notch depth equal to that of a real layered specimen; (3) under the same loading conditions to demonstrate the same critical load as that for real layered specimen. In spite of relativity of this value it is useful characteristic allowing contributions of such factors as residual stresses and material inhomogeneity to be accounted for. Thus experimental value of apparent fracture toughness of layered specimen can be found using expression (22):

$$K_{app} = Y(\alpha)\sigma_m a^{1/2}. \tag{24}$$

It follows from Eqs. (17)–(19) and (24) that apparent fracture toughness of layered composite K_{app} can be written as

$$K_{app} = [6Y(\alpha)a^{1/2}(I_{L1}^2 - I_{L0}I_{L2})(K_{lc}^{(i)} - K_r)] / \left\{ w^2 \left\{ E'_{n+1} \int_{x_n}^a h\left(\frac{x}{a}, \alpha\right) [I_{L0}x - I_{L1}] dx + \sum_{i=1}^n E'_i \int_{x_{i-1}}^i h\left(\frac{x}{a}, \alpha\right) [I_{L0}x - I_{L1}] dx \right\} \right\}, \tag{25}$$

where $K_{lc}^{(i)}$ is the fracture toughness of i th layer material.

3. Experimental

The choice of composition for Si_3N_4 based ceramics laminates is determined by the coefficient of thermal

expansion and Young’s modulus of the compounds. Three compositions of composite layers were used: (1) Si_3N_4 (M11, Starck, Germany); (2) Si_3N_4 –20 wt% TiN (grade C, Starck, Germany); (3) Si_3N_4 –30 wt% TiN (grade C, Starck, Germany). Young’s moduli, Poisson ratios and average values of coefficients of thermal expansion of the components are presented in Table 2. The more detailed information on thermomechanical parameters as well as joining temperature T_j for materials under investigation is given in [16]. Mean values of intrinsic fracture toughness of monolith materials are evaluated in the work to be approximately the same for all layer compositions, being $5 \text{ MPa m}^{1/2}$. Note that the intrinsic fracture toughness corresponds to the fracture toughness of layer material.

Milling of mixtures of certain compositions were done in the ball mill for 5 h. The formation of a thin ceramic layer is of specific importance, as the sizes of residual stress zones (tensile and compressive) are directly connected with the thickness of layers. Green tapes were manufactured with rolling. Rolling permits to control the thickness of green layers, to obtain high green density and a rather low amount of solvent and organic additives in comparison with other methods such as a tape casting [17]. However there is a problem to produce thin tapes, $<100 \mu\text{m}$, with a small amount of plasticizer and sufficient strength and elasticity to handle the green layers after rolling.

Crude rubber (4 wt%) was added to the mixture of powders as a plastisizer through a 3% solution in petrol. Then the powders were dried up to the 2 wt% residual amount of petrol in the mixture. After powders were sieved with a $500 \mu\text{m}$ sieve, granulated powders were dried up to the 0.5 wt% residual petrol. A roll mill with 40 mm rolls was used for rolling. The velocity of rolling was 1.5 m/min. Working pressure varied from 10 MPa for relative density of tapes 64% to 100 MPa for 74% density. The thickness of green tapes was either 0.4–0.5 or 0.8–1.0 mm, the width is 60–65 mm. Samples of ceramics were prepared by hot pressing of tapes stacked together. The hot pressing was performed at the temperature 1780–1820 °C, the duration 20 min and the pressure 30 MPa.

Green tapes were stacked together to form the desirable layered structure. Graphite dies were used for the hot pressing without protective atmosphere. After hot

Table 2
Thermoelastic parameters of components of layered structure

Composition	Elastic modulus (GPa)	Poisson ratio	Average value of thermal expansion coefficient ($\times 10^{-6} \text{ K}^{-1}$)
Si_3N_4	308	0.25	3
Si_3N_4 –20 wt% TiN	316	0.25	3.82
Si_3N_4 –30 wt% TiN	323	0.25	4.28

Table 3
Geometrical characteristics of $\text{Si}_3\text{N}_4/\text{Si}_3\text{N}_4\text{-X wt\% TiN}$ layered materials

Layer number	Layer composition	Layer thickness (μm)		
		$X = 20$ (specimens of type 1)	$X = 20$ (specimens of type 2)	$X = 30$ (specimens of type 3)
1	Si_3N_4	295	275	955
2	$\text{Si}_3\text{N}_4\text{-X wt\% TiN}$	315	380	355
3	Si_3N_4	260	205	175
4	$\text{Si}_3\text{N}_4\text{-X wt\% TiN}$	465	400	345
5	Si_3N_4	205	180	185
6	$\text{Si}_3\text{N}_4\text{-X wt\% TiN}$	370	285	320
7	Si_3N_4	200	230	180
8	$\text{Si}_3\text{N}_4\text{-X wt\% TiN}$	330	280	315
9	Si_3N_4	190	175	160
10	$\text{Si}_3\text{N}_4\text{-X wt\% TiN}$	370	355	380
11	Si_3N_4	180	200	–
12	$\text{Si}_3\text{N}_4\text{-X wt\% TiN}$	390	390	–
13	Si_3N_4	235	295	–
14	$\text{Si}_3\text{N}_4\text{-X wt\% TiN}$	195	175	–
15	Si_3N_4	–	175	–

pressing, the thickness of the Si_3N_4 layers was in the range of 160–960 μm , and the thickness of the Si_3N_4 layers with TiN additive varied from 160 to 480 μm . Geometrical characteristics of layered specimens are listed in Table 3.

The specimens for mechanical tests were prepared from hot pressed plates. SEVNB specimens were used for testing. The test data have confirmed that the SEVNB method can be easier applied in practice and can be used for the majority of advanced ceramics and ceramic particulate composites [18]. The V-notches with tip radii of an order of 10–15 μm were made in the specimens. Optical photograph of typical notch tip is presented in Fig. 4. The dimensions of specimens were



Fig. 4. Optical photograph of layered specimen with typical notch tip.

45 mm \times 5 mm \times 4 mm (types 1 and 2), 45 mm \times 5 mm \times 3.37 mm (type 3). The depth of the notches was about 60–80% of the specimen thickness.

A stiff load cell ensuring the rigid loading of specimens under three-point bending with a 16 mm span was used for mechanical tests. This cell is equipped with specific rigid dynamometer providing an ultimate load of 2000 N with a specimen deflection measuring system using a deflectometer suspended on the specimen. The testing machine used is designed only for the displacement of a loading crosshead and control of its speed. To study *R*-curve effect, a compliance technique was used. Notched specimen was placed into the hard load cell. Then loading of the specimen was made up to crack growth onset followed by unloading. Besides recording load-deflection diagrams, after each unloading of specimen, its polished lateral surface was examined by an optical microscope ($\times 1000$) to measure crack length. After measurement of crack length the next loading-unloading cycle was made. The operations were repeated up to total failure of specimen. Apparent fracture toughness was calculated by using of the expressions (12), (23) and (24).

4. Results and discussion

Asymmetric structure of layered specimens under study results in linear variation of residual stresses within each layer. The residual stress values calculated from thermoelastic parameters and specimen geometry using Eq. (15) are listed in Table 4. One can see that the greatest stress gradient is in laminate specimen $\text{Si}_3\text{N}_4/\text{Si}_3\text{N}_4\text{-30 wt\% TiN}$.

The critical issue to analyze fracture behavior of laminates is a choice of coordinate system. Calculated values of apparent fracture toughness K_{app} in layered

Table 4
Calculated residual stresses in Si₃N₄/Si₃N₄-X wt% TiN layered materials

Layer number	Layer composition	Residual stress ^a (MPa)		
		X = 20 (specimens of type 1)	X = 20 (specimens of type 2)	X = 30 (specimens of type 3)
1	Si ₃ N ₄	-131.7/-135.9	-157.7/-156.6	-31.3/-131.6
2	Si ₃ N ₄ -X wt% TiN	128.0/123.4	106.8/108.5	283.9/244.8
3	Si ₃ N ₄	-140.4/-144.1	-154.9/-154.1	-168.9/-187.3
4	Si ₃ N ₄ -X wt% TiN	119.6/112.8	109.4/111.1	225.5/187.5
5	Si ₃ N ₄	-150.8/-153.7	-152.4/-151.6	-223.5/-243.0
6	Si ₃ N ₄ -X wt% TiN	109.8/104.3	111.9/113.1	167.1/131.9
7	Si ₃ N ₄	-159.0/-161.8	-150.4/-149.4	-276.6/-295.5
8	Si ₃ N ₄ -X wt% TiN	101.4/96.6	114.1/115.3	112.1/77.3
9	Si ₃ N ₄	-166.5/-169.2	-148.3/-147.5	-328.6/-345.4
10	Si ₃ N ₄ -X wt% TiN	93.8/88.4	116.1/117.6	59.7/17.9
11	Si ₃ N ₄	-174.5/-177.1	-146.0/-145.2	-
12	Si ₃ N ₄ -X wt% TiN	85.8/80.0	118.5/120.2	-
13	Si ₃ N ₄	-182.7/-186.0	-143.5/-142.3	-
14	Si ₃ N ₄ -X wt% TiN	76.6/73.7	121.5/122.2	-
15	Si ₃ N ₄	-	-141.5/-140.8	-

^aResidual stresses are presented in the format “stress on low interface”/“stress on up interface”; compressive stresses are negative, tensile stresses are positive.

specimens under study are analyzed depending on crack length parameter \tilde{a} , where $\tilde{a} = Y(\alpha)a^{1/2}$. The crack length parameter \tilde{a} is the most appropriate to demonstrate critical conditions of crack growth. One of advantages of this parameter using is that stress intensity coefficient of an edge crack for fixed value of applied stress σ_m is depicted in coordinate system $K_{app} - \tilde{a}$ as a straight line from the coordinate origin. Indeed, it follows from (22) that $K_1 = \sigma_m \tilde{a}$, therefore, the slope of straight line equals to applied stress σ_m . The conditions for unstable crack growth in internal stress field are as follows [9]: $K_1(\sigma_m, a) = K_{app}(a)$; $dK_1(\sigma_m, a)/da \geq dK_{app}(a)/da$. Using parameter \tilde{a} , these conditions become: $\sigma_m \tilde{a} = K_{app}(\tilde{a})$; $\sigma_m \geq dK_{app}(\tilde{a})/d\tilde{a}$. The last two conditions can be reduced to

$$K_{app}(\tilde{a})/\tilde{a} \geq dK_{app}(\tilde{a})/d\tilde{a}. \tag{26}$$

It follows from Eq. (26) and Fig. 5 [9] that unstable crack growth occurs as the slope of straight line,

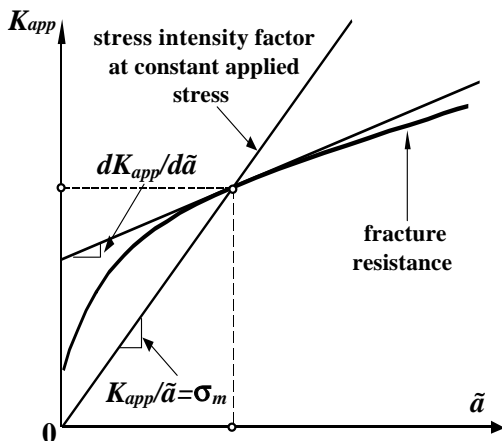


Fig. 5. Condition of unstable crack growth in internal stress field.

corresponding to stress intensity factor at constant applied stress, is no less than the slope of tangent line to fracture resistance curve at the same point.

Fig. 6 shows dependence of apparent fracture toughness on crack length parameter \tilde{a} in laminate Si₃N₄/Si₃N₄-20 wt% TiN, specimens of type 1 (solid curve). The areas corresponding to compressive and tensile layers are shown in gray and white, respectively. The fracture toughness of layer material is shown as horizontal straight line. The dependence of apparent fracture toughness on \tilde{a} is non-monotonous. The apparent fracture toughness increases in compressive layers and decreases in tensile layers. The peak values of K_{app} correspond to interfaces between layers. The apparent fracture toughness of the layered composite varies from 2 to 10 MPa m^{1/2} depending on crack length. Initial notch tip is in tenth layer that is under residual tension. Mean value of measured apparent fracture toughness corresponding to initial notch is 5.57 MPa m^{1/2} that is in accord with calculated value. Note that each experimental point in Figs. 6–8 corresponds to average value for three to five specimens. Unloading was made after small advance of crack from initial notch. Crack arrest occurred in 12th layer of specimen. The length of arrested crack was measured. Then the next loading resulted in the total failure of specimens. Mean value of measured apparent fracture toughness corresponding to arrested crack is 7.42 MPa m^{1/2} that is also in accord with calculated value.

Fig. 7 shows dependence of apparent fracture toughness on crack length parameter \tilde{a} in specimens of type 2 of laminate Si₃N₄/Si₃N₄-20 wt% TiN. Designations are the same as in Fig. 6. The dependence of apparent fracture toughness on crack length parameter is non-monotonous also. The fracture toughness behavior

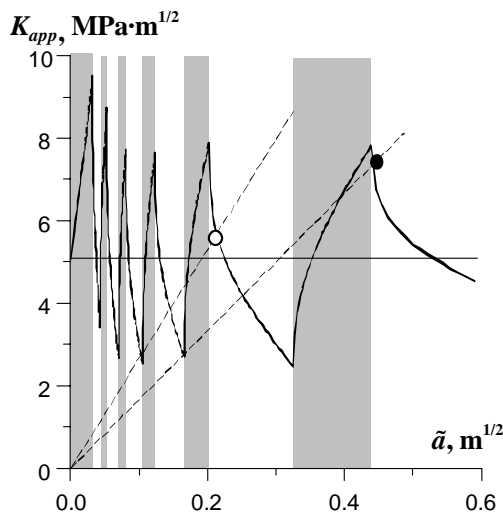


Fig. 6. Dependence of apparent fracture toughness on crack length parameter \tilde{a} in laminate $\text{Si}_3\text{N}_4/\text{Si}_3\text{N}_4$ -20 wt% TiN (specimens of type 1). Areas of compressive layer are shown in grey. Solid curve is the calculated dependence, horizontal line is the fracture toughness of layer material. Dashed line is the stress intensity factor at constant applied stress of crack growth onset. Open circle corresponds to initial notch, filled circle corresponds to arrested crack.

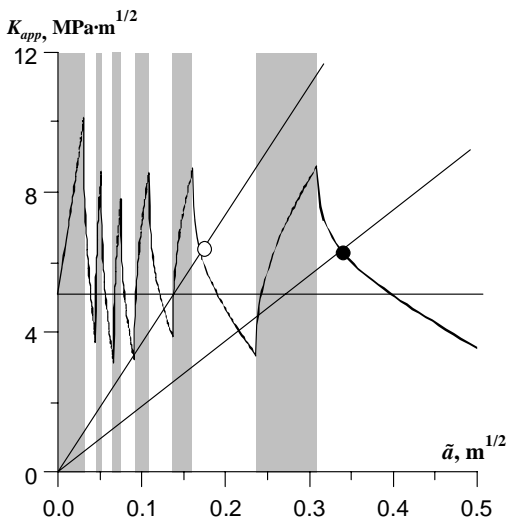


Fig. 7. Dependence of apparent fracture toughness on crack length parameter \tilde{a} in laminate $\text{Si}_3\text{N}_4/\text{Si}_3\text{N}_4$ -20 wt% TiN (specimens of type 2). Designations are the same as in Fig. 6.

in compressive and tensile layers in specimens of type 2 is qualitatively similar to that in specimens of type 1. However, difference of specimens geometry results in some difference of apparent fracture toughness range. Specifically the apparent fracture toughness of specimens of type 2 varies from 3 to 11 MPa·m^{1/2}. Initial notch tip in the specimen is also in tenth layer that is under residual tension. In this case mean value of measured apparent fracture toughness corresponding to initial notch is 6.39 MPa·m^{1/2}. That is in accord with

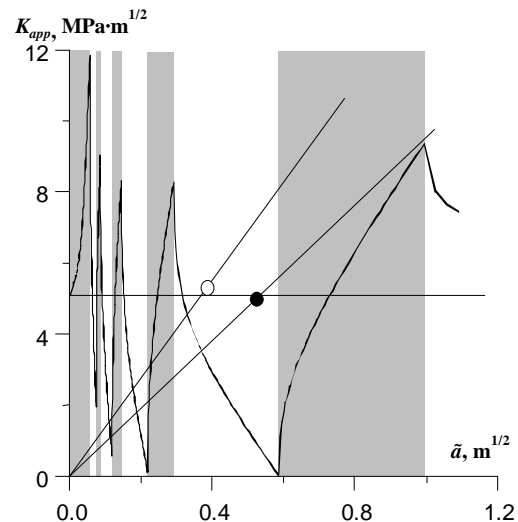


Fig. 8. Dependence of apparent fracture toughness on crack length parameter \tilde{a} in laminate $\text{Si}_3\text{N}_4/\text{Si}_3\text{N}_4$ -30 wt% TiN (specimens of type 3). Designations are the same as in Fig. 6.

calculated value too. After unloading crack was arrested in 12th layer like specimens of type 1. Specimens of type 2 with arrested crack demonstrate the apparent fracture toughness value of 6.27 MPa·m^{1/2}. This is in good accord with calculated value.

Fig. 8 shows dependence of apparent fracture toughness on crack length parameter \tilde{a} for the laminate $\text{Si}_3\text{N}_4/\text{Si}_3\text{N}_4$ -30 wt% TiN (specimens of type 3). Designations are also the same as in Figs. 6 and 7. In this case we have non-monotonous dependence too. Apparent fracture toughness range in Fig. 8 is more wide and different from range of $\text{Si}_3\text{N}_4/\text{Si}_3\text{N}_4$ -20 wt% TiN laminate due to differences of composition and geometry. The apparent fracture toughness of $\text{Si}_3\text{N}_4/\text{Si}_3\text{N}_4$ -30 wt% TiN laminate varies from 0.1 to 12 MPa·m^{1/2}. Initial notch tip in the specimen is in eighth layer that is under residual tension. The mean value of measured apparent fracture toughness corresponding to initial notch is 5.31 MPa·m^{1/2}. After unloading crack was arrested in the same (8th) layer. $\text{Si}_3\text{N}_4/\text{Si}_3\text{N}_4$ -30 wt% TiN specimens with arrested crack demonstrate the apparent fracture toughness value of 5 MPa·m^{1/2}. In contrast to $\text{Si}_3\text{N}_4/\text{Si}_3\text{N}_4$ -20 wt% TiN layered specimens, there is essential difference of experimental and calculated apparent fracture values. Specifically, mean apparent fracture toughness, corresponding to initial notch, exceeds the calculated value by 2.1 MPa·m^{1/2}. The mean apparent fracture toughness, corresponding to arrested crack, exceeds the calculated value by 4 MPa·m^{1/2}. The difference can be associated with existence of stable crack growth in compressive layer following the layer containing notch tip. An explanation of the difference between experimental and theoretical values of fracture toughness of layered specimens studied is considered elsewhere [16].

Let consider some features of crack arresting in our experiments. Open circle A in Fig. 9 designates the initial state of testing: initial notch without loading. Open circle B corresponds to the crack growth onset at some critical applied stress. Open circles depict the initial notch with length a_0 . Filled circle C corresponds to the onset of unloading. Note that the applied stress increases permanently during loading stage (from A to C in Fig. 9), while the crack begins to grow only as applied stress intensity factor becomes more than apparent fracture toughness (from B to C in Fig. 9). The crack growth under unloading can vary depending on the rate of applied stress decreasing. Schematically it is shown in Fig. 9 by two ways of crack development (C–D–E–F, Fig. 9(a); C–D'–E'–F', Fig. 9(b)). The curve C–D'–E'–F' corresponds to greater rate of applied stress falling. Filled circles D and D' characterize current positions of moving crack tip under unloading. Filled circles E and E' designate the crack arresting when applied crack intensity factor becomes less than apparent fracture toughness. Filled circles F and F' depict the final state of crack with length a_f (or a'_f) after full unloading. One can see from Fig. 9 that different conditions of unloading can result in various distance passed by the crack. If C–D–E–F way is realized, the crack is arrested in next tensile layer (Fig. 9(a)). If C–D'–E'–F' way is realized the crack is arrested in the nearest compressive layer (Fig. 9b). In general case, unloading conditions can result in many different final positions of crack tip. It can be either in layer with initial notch tip or in any more remote layer. Returning to our experimental data we note that rather C–D–E–F way than C–D'–E'–F' is realized in the laminate specimens containing 20% TiN in tensile layers. At the same time the specimens with 30% TiN in tensile layers demonstrate C–D'–E'–F' way at unloading, which may be associated with existence of stable crack growth in compressive layer following the layer containing notch tip. The problem will be analyzed elsewhere [16].

In such a way we have two stages of loading process and three stages of crack behavior. First stage of loading process is the applied stress increasing to some maximum value (from A to C in Fig. 9(a)). Second stage of loading process is the applied stress decreasing up to zero (from C to F in Fig. 9(a)). First stage of crack behavior is the absence of crack growth until applied stress intensity factor is less than apparent fracture toughness (from A to B in Fig. 9(a)). Second stage of crack behavior is the crack growth (from B to E in Fig. 9(a)). Third stage of crack behavior is the absence of crack growth as applied stress intensity factor is less than apparent fracture toughness again (from E to F in Fig. 9(a)).

The condition for stable crack growth in residually stressed layers can be obtained from (26). The stable crack growth can occur when $K_{app}(\tilde{a})/\tilde{a} < dK_{app}(\tilde{a})/d\tilde{a}$.

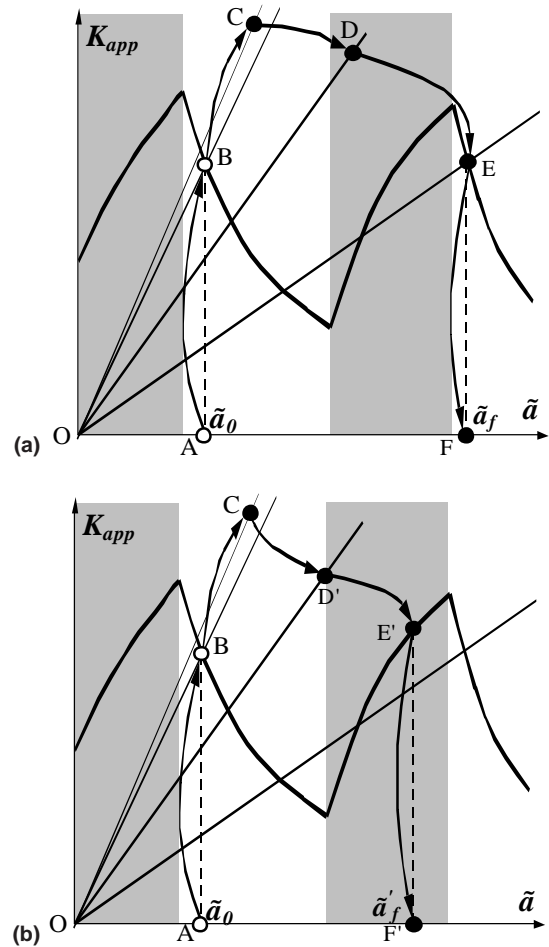


Fig. 9. Stages of crack arresting in layered specimen: (a) crack is arrested in tensile layer; (b) crack is arrested in compressive layer.

As the condition is fulfilled load decreasing results in indispensable crack arresting. The crack arresting in stable growth condition differs from features of crack arresting being in our work. This is due to the fact that unstable crack growth was observed for the layered specimens investigated. Crack arresting does not depend upon unloading rate in conditions of stable crack growth. Crack will be arrested in any case as applied load does not increase. At the same time crack arresting for unstable crack growth is dependent strongly on stress decreasing rate. The unloading rate is determined mainly by stiffness of loading cell. The more is the stiffness the less is crack path before arresting. It is evident that stable crack growth will lead to strengthening and an insensitivity of strength to the initial flaw size. In a layered material design process it is necessary to determine the range of stable crack growth and strengthening if the range of flaws in layers is known. Usually technological flaws are relatively small in laminates. Only rising dependence of apparent fracture toughness on crack length is not enough to obtain desirable strengthening and toughening. The dependence is

effective in imparting flaw tolerance only if the slope of the apparent fracture toughness curve is steep at short crack lengths. Obtaining high residual compressive stress is an effective way to provide high toughness at small crack lengths, thereby ensuring flaw tolerance and surface damage resistance.

A key issue of the mechanical behavior of layered composites is an effect of their apparent fracture toughness on strength properties and reliability. As was shown above the crack instability criterion involves the point of tangency between the applied (crack driving) stress intensity factor and the apparent fracture toughness curve. It is only beyond the tangency point that unstable crack propagation occurs, leading to catastrophic failure. A unique material toughness parameter, K_{1c} , no longer controls the applied stress at which fracture occurs; it is the exact form of the K_{app} curve, $K_{app}(a)$, that determines the fracture stress of a layered material. The residual stresses distribution is superimposed upon the strength behavior of layered composites. Residual stress as well as initial cracks have essential effect on fracture stress. For instance, it was shown in [19,20] that the strength of the three-layer Al_2O_3 –15 vol% ZrO_2 composite with residual stress was about 500 MPa greater than those of monolithic ceramic. One can suppose that, in case of crack growth, residual stress affects laminate strength in more complicated manner as compared to simple superposition of stresses.

It is of interest to compare how the stress required to grow a crack of a given length differed from what would be required to grow the crack in the monolith minus the internal stress in the layer where the crack tip lies. For example, calculation results to compare the behavior of these stresses in specimens of type 2 depending on relative crack length a/w are shown in

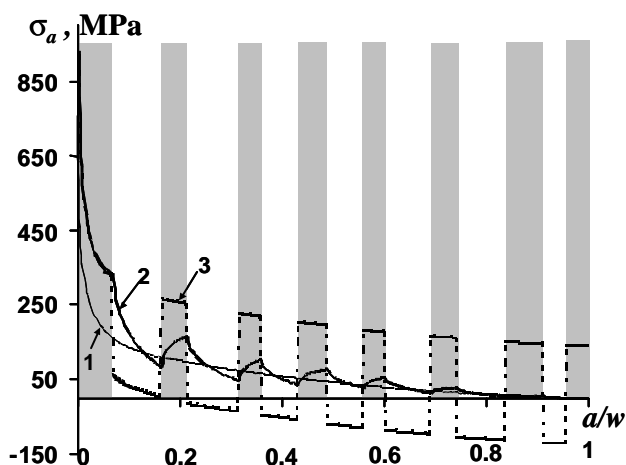


Fig. 10. Stresses required for crack growth vs crack length. 1 is the crack growth stress in monolithic material; 2 is the fracture stress of the layered material; 3 is the superposition of the crack growth stress in monolithic material and residual stresses in layers.

Fig. 10. Curve 1 corresponds to the crack growth stress in monolithic material calculated as fracture toughness of the material divided by crack length parameter. Curve 2 is the fracture stress of the layered material calculated from (24). Curve 3 is the superposition of the crack growth stress in monolithic material and residual stresses in layers. One can see that in first layer the difference of the stresses depicted by curves 2 and 3 is small. In other words, for the first layer the difference of fracture stress for the monolith and that for the laminate practically equals absolute value of residual stress in this layer.

In the next layers the stresses corresponded to curves 2 and 3 differ substantially. Note that the fracture stress magnitudes depicted by curve 3 can be negative for tensile layers. This is due to the fact that tensile residual stress is more than the fracture stress for monolithic material if crack is too long. It means that simple superposition is not valid for long cracks crossing several layers.

5. Conclusions

The toughening of ceramic matrix asymmetric laminates with elastic inhomogeneity has been studied both analytically and experimentally. Applied and residual stress distributions are determined for arbitrary alteration of different layers. Expression for apparent fracture toughness of residually stressed asymmetric layered material is obtained. The most appropriate coordinate system to analyze fracture conditions of laminar composite was shown to be the system where apparent fracture toughness is depicted depending on crack length parameter $\tilde{a} = Y(x)a^{1/2}$. The dependences of apparent fracture toughness on crack length parameter are calculated for the specimens tested. Conditions of crack arresting, stable and unstable crack growth in layered structure are analyzed. It was shown that the crack path before arresting can vary depending on stiffness of loading cell. Experimental values of apparent fracture toughness were measured with compliance technique. They are in good agreement with calculation data.

Acknowledgements

The work was supported with European Commission. It is part of the Project “Silicon nitride based laminar and functionally gradient ceramics for engineering application”, Proposal No. 1CA2-1999-10109, Contract No. 1CA2-CT-2000-10020, the program Copernicus – 2. The authors thank also V. Galenko and B. Ozersky for their help during the course of this work.

References

- [1] Chan M. Layered ceramics: processing and mechanical behavior. *Annu Rev Mater Sci* 1997;27:249–82.
- [2] Clegg WJ, Kendall K, Alford NM, Button TW, Birchall JD. A simple way to make tough ceramics. *Nature* 1990;347:455–7.
- [3] Lakshminarayanan R, Shetty DK, Cutler RA. Toughening of layered ceramic composites with residual surface compression. *J Am Ceram Soc* 1996;79(1):79–87.
- [4] Lugovy M, Orlovskaya N, Slyunyayev V, Gogotsi G, Kuebler J, Sanchez-Herencia AJ. Crack bifurcation features in laminar specimens with fixed total thickness. *Compos Sci Technol* 2002;62:819–30.
- [5] Marshall DB, Ratto JJ, Lange FF. Enhanced fracture toughness in layered microcomposites of CeO–ZrO₂ and Al₂O₃. *J Am Ceram Soc* 1991;74(12):2979–87.
- [6] Lugovy M, Orlovskaya N, Berroth K, Kuebler J. Macrostructural engineering of ceramic-matrix layered composites. *Compos Sci Technol* 1999;59:1429–37.
- [7] Blattner AJ, Lakshminarayanan R, Shetty DK. Toughening of layered ceramic composites with residual surface compression: effects of layer thickness. *Eng Fract Mech* 2001;68:1–7.
- [8] Evans AG. Perspective on the development of high-toughness ceramics. *J Am Ceram Soc* 1990;73(2):187–206.
- [9] Sglavo VM, Larentis L, Green DJ. Flaw-insensitive ion-exchanged glass: I, theoretical aspects. *J Am Ceram Soc* 2001;84(8):1827–31.
- [10] Moon RJ, Hoffman M, Hilden J, Bowman K, Trumble K, Roedel J. Weight function analysis on the *R*-curve behavior of multilayered alumina–zirconia composites. *J Am Ceram Soc* 2002;85(6):1505–11.
- [11] Fett T, Munz D. Influence of crack-surface interactions on stress intensity factor in ceramics. *J Mater Sci Lett* 1990;9:1403–6.
- [12] Timoshenko SP, Goodier JN. *Theory of elasticity*. 3rd ed. New York: McGraw-Hill; 1970.
- [13] Giannakopoulos AE, Suresh S, Finot M, Olsson M. Elastoplastic analysis of thermal cycling: layered materials with compositional gradients. *Acta Metall Mater* 1995;43(4):1335–54.
- [14] Sergo V, Lipkin DM, De Portu G, Clarke DR. Edge stresses in alumina/zirconia laminate. *J Am Ceram Soc* 1997;80(7):1633–8.
- [15] Srawley JE. Wide range stress intensity factor expressions for ASTM E 399 standard fracture toughness specimens. *Int J Fract* 1976;12:475–6.
- [16] Lugovy M, Slyunyayev V, Orlovskaya N, Blugan G, Kuebler J, Lewis M. Apparent fracture toughness of Si₃N₄-based laminates with residual compressive or tensile stresses in surface layers. *Acta Mater* [submitted].
- [17] Hyatt T. Electronics: tape casting, roll compaction. *Am Ceram Soc Bull* 1995;74:56–9.
- [18] Gogotsi GA. Fracture toughness studies on ceramics and ceramic particulate composites at different temperatures. In: Salem JA, Quinn GD, Jenkins MG, editors. *Fracture resistance testing of monolithic and composite brittle materials ASTM STP 1409*. West Conshohocken (PA): American Society for Testing and Materials; 2002. p. 199–212.
- [19] Hansen J, Cutler RA, Shetty DK, Virkar AV. Indentation fracture response and damage resistance of Al₂O₃–ZrO₂ composites strengthened by transformation-induced residual stresses. *J Am Ceram Soc* 1988;71(12):C-501–5.
- [20] Cutler RA, Bright JD, Virkar AV, Shetty DK. Strength improvement in transformation toughened alumina by selective phase transformation. *J Am Ceram Soc* 1987;70(10):714–8.